

The Deuterium to Hydrogen Abundance Ratio Towards a Fourth QSO: HS 0105+1619

John M. O'Meara^{1,2}, David Tytler^{1,3},
David Kirkman⁴, Nao Suzuki⁵, Jason X. Prochaska^{1,6}, Dan Lubin⁷ & Arthur M. Wolfe⁸
Center for Astrophysics and Space Sciences;
University of California, San Diego;
MS 0424; La Jolla; CA 92093-0424

ABSTRACT

We report the measurement of the primordial D/H abundance ratio towards QSO HS 0105+1619. The column density of the neutral hydrogen in the $z \simeq 2.536$ Lyman limit system is high, $\log N_{HI} = 19.422 \pm 0.009 \text{ cm}^{-2}$, allowing for the deuterium to be seen in 5 Lyman series transitions. The measured value of the D/H ratio towards QSO HS 0105+1619 is found to be $D/H = 2.54 \pm 0.23 \times 10^{-5}$. The metallicity of the system showing D/H is found to be $\simeq 0.01$ solar, indicating that the measured D/H is the primordial D/H within the measurement errors. The gas which shows D/H is neutral, unlike previous D/H systems which were more highly ionized. Thus, the determination of the D/H ratio becomes more secure since we are measuring it in different astrophysical environments, but the error is larger because we now see more dispersion between measurements. Combined with prior measurements of D/H, the best D/H ratio is now $D/H = 3.0 \pm 0.4 \times 10^{-5}$, which is 10% lower than the previous value. The new values for the baryon-to-photon ratio, and baryonic matter density derived from D/H are $\eta = 5.6 \pm 0.5 \times 10^{-10}$ and $\Omega_b h^2 = 0.0205 \pm 0.0018$ respectively.

¹Visiting Astronomer, W.M. Keck Observatory which is a joint facility of the University of California, the California Institute of Technology and NASA.

²E-mail: jomeara@ucsd.edu

³E-mail: tytler@ucsd.edu

⁴E-mail: david@mamacass.ucsd.edu

⁵E-mail: suzuki@ucsd.edu

⁶E-mail: xavier@ociw.edu, Observatories of the Carnegie Institute of Washington

⁷E-mail: dlubin@ucsd.edu

⁸E-mail: awolfe@ucsd.edu

Subject headings: quasars: absorption lines – quasars: individual
(HS 0105+1619) – cosmology: observations

1. Introduction

The standard theory of big bang nucleosynthesis (SBBN) predicts the abundances of the light nuclei H, D, ^3He , ^4He , and ^7Li as a function of the cosmological baryon to photon ratio, $\eta = n_b/n_\gamma$ (Kolb & Turner 1990; Walker et al. 1991; Schramm & Turner 1998; Nollett & Burles 2000; Olive, Steigman & Walker 2000). A measurement of the ratio of any two primordial abundances gives η , and hence the baryon density, while a second ratio tests the theory. However, it is extremely difficult to measure primordial abundances, because in most places gas ejected from stars has changed the abundances.

Adams (1976) suggested that it might be possible to measure the primordial D/H ratio in absorption line systems towards QSOs. Although gas which has been inside a star will have lost all of its deuterium, in QSO absorption line systems having typical metal abundances of 0.001 to 0.01 of the solar value, about 0.1 – 1% of the deuterium will have been lost.

The advent of the HIRES spectrograph (Vogt 1994) on the W.M. Keck-I telescope gave the high signal-to-noise ratio (SNR) and spectral resolution needed to reveal deuterium (Tytler et al. 2000) in high redshift absorption systems. We have previously measured D/H in two QSOs (Tytler, Fan & Burles 1996; Tytler & Burles 1997; Burles & Tytler 1998a; Burles & Tytler 1998b), and placed a strong upper limit on D/H in a third (Kirkman et al. 1999).

Other QSOs give less useful constraints on D/H, because their absorption systems are more complex, or existing spectra are inadequate. The Lyman limit system (LLS) at $z_{abs} = 0.701$ towards QSO PG 1718+4807 might allow ten times larger D/H, or it may give no useful constraints (Webb et al. 1997; Levshakov, Kegel, & Takahara 1998; Tytler et al. 1999). Molaro et al. (1999) claimed another QSO absorption system showed low D/H, but they and Levshakov et al. (2000) note that since only the Ly α line has been observed, the hydrogen velocity structure and the H I column density are poorly known, and the deuterium feature can be fit using hydrogen alone.

In this paper, we present a fourth QSO, HS 0105+1619, which gives strong constraints on the primordial D/H ratio.

2. Observations and data reduction

We report the detection of deuterium in the QSO HS 0105+1619 (emission line redshift 2.64, $V=16.9$, B1950 RA 1h 5m 26.97s, DEC +16d 19m 50.1s; J2000 RA 1h 8m 6.4s, DEC +16d 35m 50.0s), which was discovered by Hagen, Engels & Reimers (1999), who very kindly gave us a finding chart and a low resolution spectrum prior to publication.

We present high quality, high SNR spectra of HS 0105+1619 in both low and high resolution. The low resolution spectra were obtained using the Kast double spectrograph on the Shane 3 meter telescope at Lick observatory. The high resolution spectra were obtained using the HIRES spectrograph on the Keck-I telescope. The observations are summarized in Table 1. All of the high resolution observations were taken using the HIRES image rotator to align the direction of atmospheric dispersion along the slit, and were taken with the C5 decker, which provides an entrance aperture to the spectrograph with dimensions $1.15'' \times 7.5''$. The spectra were sampled in 2.1 km s^{-1} pixels with the Tektronix 2048x2048 CCD.

The HIRES spectra were flat-fielded, optimally extracted, and wavelength calibrated using Tom Barlow’s set of echelle extraction MAKEE programs. The spectra were then co-added to produce a single spectrum. This spectrum was then flux calibrated using the low resolution Kast spectrum. Because the SNR decreases in both spectra at lower wavelengths, we use the flux calibrated data for wavelengths greater than 3800 \AA and the co-added spectrum without flux calibration below 3800 \AA . The details regarding the co-adding and fluxing are given in Suzuki & Tytler (2000). The wavelength scale has an external zero point error of approximately $\pm 10 \text{ km s}^{-1}$, which is the shift between spectra taken at different times, which we corrected. The internal error in the wavelength scale is a least 0.09 km s^{-1} , from the arc line fits, and may be approximately $1 - 2 \text{ km s}^{-1}$, which is the size of the error which we have noted in our analysis of other similar spectra (Levshakov, Tytler & Burles 2000). The final spectrum has 2.1 km s^{-1} wide pixels, and a SNR of approximately 80 and 10 at the Ly α and Lyman limit of the D/H system, respectively. In Figure 1, we show the flux calibrated Kast and HIRES spectra.

3. General Properties of the $z \simeq 2.536$ Lyman Limit System Towards HS 0105+1619

As can be seen in Figure 1, the low resolution Kast spectrum of HS 0105+1619 shows a steep Lyman break at a wavelength of approximately 3230 \AA , which is

caused by a Lyman limit system at a redshift of $z \simeq 2.54$. At this redshift we see a strong Ly α absorption line, near 4300 Å. Our analysis of the high resolution HIRES spectrum indicates that there is a Lyman limit system at a redshift of $z \simeq 2.536$, which shows deuterium and numerous metal absorption lines. We discuss the general features of the absorption below, and the best fits to the data in the following section.

3.1. Hydrogen Absorption

We observe hydrogen in all Lyman series transitions through Lyman-17, where the spectrum abruptly ends at 3233 Å due to line blending near the Lyman limit. The observed Lyman transitions are shown in Figure 2.

The column density of the hydrogen is high, as Figure 2 indicates. All of the Lyman series transitions are saturated through to the Lyman limit, indicating that the column density is at least $\log N_{HI} \geq 17.8 \text{ cm}^{-2}$. The Ly α line has zero flux across about 200 km s $^{-1}$ indicating that the column density of the system is approaching the levels found in damped Ly α systems.

Inspection of Figure 2 also indicates that the absorption system is very simple. The Ly-5, Ly-6, Ly-7, Ly-9, Ly-10, Ly-14, and Ly-15 transitions all appear symmetric and un-blended, allowing us to describe the absorber by a single component.

3.2. Deuterium Absorption

Since the column density of the hydrogen responsible for the Lyman limit appears high, we expect the associated deuterium absorption to be strong. For the first time, we observe absorption at the predicted position of deuterium, a velocity of $v = -81.64 \text{ km s}^{-1}$ in the frame of the H I, in 5 Lyman series transitions: Ly β , Ly γ , Ly-5, Ly-6, and Ly-7. Deuterium Ly α was not observed since it is subsumed by the absorption of the hydrogen Ly α , and deuterium Ly-4 was not observed due to intervening Ly α forest absorption.

The observed absorption is narrow, and appears symmetric and free of strong contamination, suggesting that like the hydrogen, the absorption is simple and can be modeled with a single component.

In all transitions where absorption is observed, the velocity of the absorption appears centered about the same value, $v \simeq -82 \text{ km s}^{-1}$, strongly indicating that the features are all Lyman transitions of the same absorber, and that the absorber is consistent with being deuterium. In a later section, we give a more

rigorous discussion of why we believe the absorption is indeed deuterium, and not hydrogen or other ions.

3.3. Metal Line Absorption

The $z \simeq 2.536$ Lyman limit system shows a variety of metal ions, as seen in Figure 3. Unlike Lyman Limit systems with column densities in the range of $\log N_{HI} = 16.5\text{--}18 \text{ cm}^{-2}$ which show absorption predominantly in the higher ionization states, this system shows metal line absorption in neutral, low, and high ionization states. Since the column density of the hydrogen appears high, we expect the neutral and low ionization metal lines to trace the H I, and with it the deuterium, in analogy with damped Ly α systems.

All of the low ionization metal lines are extremely narrow, and appear to be well described by a single component. Moreover, the low ions are all centered at $v \simeq 0 \text{ km s}^{-1}$, implying that they arise in the same gas as the H I and D I.

4. Best Parameters for the $z \simeq 2.536$ Lyman Limit System

We now give the parameters which describe the absorption in the $z \simeq 2.536$ Lyman Limit system towards HS 0105+1619. For all measurements, a continuum was fit to the region under consideration to produce a unit normalized spectrum. The observed absorption features were then fit using the VPFIT Voigt profile line-fitting routine (Webb, 1987; kindly provided by Carswell) and re-verified using in-house routines. For each absorber, we obtain an estimate of the column density, N , the redshift, z , and the velocity width, b , along with their respective 1σ errors. The results of this analysis are found in Table 2.

4.1. The Hydrogen

The parameters describing the hydrogen absorption responsible for the Lyman limit are obtained from various complementary parts of the spectrum, and are given by $\log N_{HI} = 19.422 \pm 0.009 \text{ cm}^{-2}$, $b = 13.99 \pm 0.20 \text{ km s}^{-1}$, and $z = 2.535998 \pm 0.000007$.

The deuterium and low ionization metal absorption lines give a strong indication that the H I can be modeled by a single component, whose redshift should be consistent with that of the other neutral ions observed, namely O I and N I. We find that a single component fit allows for an excellent description of the observed absorption, and we now consider the individual parameters.

4.1.1. Redshift

The redshift of the hydrogen was determined by simultaneously fitting the Lyman series absorption at Ly α , Ly β , Ly γ , Ly-5, Ly-6, Ly-7, Ly-9, Ly-10, Ly-13, Ly-14, and Ly-15.

4.1.2. Velocity Width

The high column density of the absorber does not give us information on the velocity width at Ly α , so we must turn to the higher order Lyman series lines. To determine b , we fit the absorption in the Lyman series in transitions which appear to be least contaminated by interloping Ly α forest, specifically Ly-9, Ly-10, Ly-14, and Ly-15, simultaneously. The inclusion of all observed Lyman series transitions in the fitting procedure does not change the measured b value.

4.1.3. Column Density

Three regions of the spectrum allow us to determine the column density: the Lyman limit, the core of the Ly α , and the damping wings of the Ly α . These regions are shown in Figure 4 along with the single component best fit to the H I.

The Lyman limit allows for a lower limit to the column density of the hydrogen of $\log N_{HI} = 17.8 \text{ cm}^{-2}$ since all observed Lyman series lines observed are saturated.

The Ly α line gives the most information regarding the hydrogen column density, because it is insensitive to the b value, even though it is sensitive to the continuum level. In Figure 5, we show the continuum used to fit the 250 Å region encompassing Ly α and the corresponding approximate 1σ levels, which amount to a $\pm 2\%$ continuum level change. To determine the effect of the continuum placement on the measured value on the column density, for all regions of the Ly α line, we obtain a fit using the best continuum estimate, and then move the continuum to the $\pm 1\sigma$ levels and re-fit. In all fits to the Ly α , we choose segments of the spectra which appear to be least contaminated by other absorption.

In Figure 6, we show the fit to the core of $\log N_{HI} = 19.419 \pm 0.009 \text{ cm}^{-2}$, where the error is the quadratic sum of the error from the continuum (0.007) and the error from the fit (0.006). This fit was made for two regions on either side of the line center: 4294.5–4295.5 and 4300–4302 Å. There is additional

absorption in the core between 4295.5 and 4297 Å which is readily fit by two H I Ly α lines. Their absorption is seen and fit in Ly β , but they contribute no significant optical depth to the lower wavelength (4294.5–4295.5 Å) region which gives the column density of the H I which shows deuterium.

We note that contamination of the core region is possible, and would lower the measured column density. However, we consider such contamination unlikely, since it would require at least two lines appearing in the right places, with a very restricted set of parameters, to produce enough absorption to fit both sides of the core region.

The damping wings of the Ly α absorber also give the column density, but the exact continuum placement is now the dominant source of error because the continuum uncertainty represents a larger fraction of the total absorption in these regions. Two damping wing regions were fit, one on either side of the line center. On the blue (lower wavelength) side, we fit the wavelengths 4288.4–4289.3 Å, which gave $\log N_{HI} = 19.406 \pm 0.060 \text{ cm}^{-2}$, where the errors are the range in column density allowed by the $\pm 2\%$ range in the continuum placement. For the red (higher wavelength) side regions 4306–4307 and 4308–4309 Å were fit giving $\log N_{HI} = 19.4752 \pm 0.040 \text{ cm}^{-2}$.

For our best value for the H I column density, we take the weighted mean of the three measurements from the core and wings: $\log N_{HI} = 19.422 \pm 0.009 \text{ cm}^{-2}$. All three estimates of the column density are consistent with this mean.

4.2. The Deuterium

The determination of the parameters describing the deuterium absorption is relatively straightforward, given the presence of 5 un-blended transitions, most of which are unsaturated. We begin by fitting the D I transitions, and then assess possible sources of error.

The D I transitions are well fit by an absorber with $\log N_{DI} = 14.810 \pm 0.029 \text{ cm}^{-2}$ and a velocity width of $b = 9.93 \pm 0.29 \text{ km s}^{-1}$. This fit is shown in Figure 7. These values were determined by fitting the regions surrounding the deuterium in all 5 deuterium absorption regions simultaneously, with the redshift of the deuterium tied to the hydrogen, and the parameters for the hydrogen absorption fixed at $\log N_{HI} = 19.42 \text{ cm}^{-2}$ and $b = 13.99 \text{ km s}^{-1}$. In all fits, the regions used to fit deuterium were constrained to be those within approximately -150 and $+20 \text{ km s}^{-1}$ of the H I line center, and are listed in Table 3. Where needed, additional Ly α forest absorption was fit to model all absorption. The parameters for the additional lines are given in table 4.

The uncertainty in the continuum level increases the error on the D I column density by a third. Independent estimates of the continuum levels at the D I transitions had a 1σ dispersion of approximately 10% , much larger than the 2% error near Ly α , where the data has been flux calibrated and has significantly higher SNR. To gauge the effect on the error in the D I column density, we determined the parameters of the deuterium absorption independently for each line, both for the best estimate of the continuum and for a 10% higher continuum level. The difference between these two is the contribution to the error from the choice of continuum level. For each each D I transition, this error was added in quadrature to the error obtained with the best continuum. The weighted mean for the five D I transitions gives $\log N_{DI} = 14.826 \pm 0.039 \text{ cm}^{-2}$ and $b = 9.85 \pm 0.42 \text{ km s}^{-1}$. The results of the independent fits to the different deuterium transitions with the best estimate of the continuum level can be seen in Figure 8.

The error on $\log N_{DI}$ is insensitive to a change in the redshift of 1 km s^{-1} , as found by both letting the deuterium fit freely to its own redshift, and by tying the redshift to the H at 1 km s^{-1} away from the best fit value. Both results gave a $\log N_{DI}$ which deviated by amounts significantly lower than the best fit 1σ errors.

The effect of varying the main hydrogen by the 1σ errors in either column density or velocity width produced no effective change on the $\log N_{DI}$ since the main hydrogen component is well separated from the deuterium because the b of the hydrogen is very small.

4.3. The Metals

The results of fits to the many metal lines are given in Table 2, and a subset of the fits is shown in Figure 9. In all cases, the ions were best fit by a single component whose redshift, velocity width, and column density were all allowed to vary. Many of these ions show multiple transitions, and for any single ion, all transitions present in the spectra were fit simultaneously.

The metals were all found to lie within 8 km s^{-1} of the redshift of the hydrogen which shows deuterium. More importantly, since the column density of the hydrogen is so high, we expect the redshifts of the low and neutral ions to agree with the hydrogen since we expect the gas to be predominantly neutral. The neutral and singly ionized ions agree with the hydrogen redshift to within 2 km s^{-1} , while the neutral ions alone, in the top section of Table 2, agree to within approximately 1 km s^{-1} . The larger dispersion seen for the singly

ionized ions, in the second section of the table, indicates that some of the gas making these lines is distinct from the neutral gas, but this dispersion could be insignificant, because the internal wavelength errors could be 1–2 km s⁻¹.

The detection of O I is of particular importance in this system for two reasons. First, the ionization potential of O I is nearly identical to that of hydrogen, so it is ionized by the same photons that ionize the H I. Second, O I participates in electron transfer with H I, such that in cases where the gas is not highly ionized, O I/O is nearly identical to H I/H, and the distribution of O I should match that of the H I and the D I. The O I absorption gives information about the temperature, bulk motion, ionization and abundances in the neutral gas which shows the D I absorption. Since the O I is accurately modeled by a single, narrow component in four separate transitions, we gain confidence that a single component fit to the deuterium and to the hydrogen is sufficient. The implications of the measurement of O I on the metallicity and ionization are discussed in a later section.

Since O I and H I should arise in the same gas, we use these lines to obtain the temperature of the gas which shows D I and its turbulent velocity. We model the observed b as $b^2 = b_{inst}^2 + b_{int}^2$. The instrument line broadening, b_{inst}^2 was measured from arc lamp calibration spectra to be $b_{inst} = 4.81 \pm 0.14$ km s⁻¹. We model the intrinsic velocity width as $b_{int}^2 = b_{temp}^2 + b_{turb}^2$; a combination of thermal broadening and bulk motion. The thermal broadening, $b_{temp}^2 = 2kT/m = 166.41(T/10^4\text{K})/\text{mass}(\text{amu})$, depends on the ion mass in atomic units, m , but the b_{turb} is the same for all ions. All of the b values quoted in this paper and listed in Table 2 refer to intrinsic line widths, but the listed errors do not include the error in b_{inst} , because we do not know whether this error is correlated at different wavelengths.

Fitting O I, N I and H I alone gives $T = 1.15 \pm 0.02 \times 10^4$ K, and $b_{turb} = 2.56 \pm 0.12$ km s⁻¹, which we show by the straight line in Figure 10. The errors quoted here are very much minimum values, because they do not include the error in the b_{inst} or the appropriateness of the model.

Ions C II, Si II and Fe II, are all wider than predicted by this fit, presumably because a part of each line arises in gas with different velocity structure. The lines from the higher ionization ions C III, C IV, N II, Si III and Si IV have velocities which differ by 0 to –7 km s⁻¹ from the H I and low ionization ions. They are not relevant to the D/H because their ionization and velocities show that they arise in different gas, a common finding for absorption systems with high N_{HI} (Wolfe & Prochaska 2000a), but unlike absorption systems with much lower N_{HI} , including PKS 1937–1009 and Q1009+2956.

5. Is the Observed Absorption Deuterium?

Now that we have determined the parameters of the absorption at the position of deuterium, we turn to the issue of confirming that the absorption is indeed deuterium, and not inter-lopings hydrogen or metal line contamination.

The primary concern with the absorption seen at the position of deuterium would be that it is caused not by deuterium, but instead by inter-lopings hydrogen. Here we argue that this scenario is unlikely for the following reasons.

First, hydrogen lines in the Ly α forest with the appropriate column density, $\log N_{HI} \simeq 14.8 \text{ cm}^{-2}$ have $b > 20 \text{ km s}^{-1}$, and not $b \simeq 10 \text{ km s}^{-1}$ (Kim et al. 1997; Kirkman & Tytler, 1997). However, such low values of b might be found in components of the LLS, which are the most likely contaminants. Second, we are able to predict the width of the deuterium using the measured widths of the other neutral ions observed which are present in the same gas. Figure 10 illustrates the concept. Since we have observed three other neutral ions (H I, O I, N I), we can use their widths to predict the width of deuterium. As Figure 10 shows, the measured value of $b(D)$ is consistent with its predicted value. Third, hydrogen lines with a $\log N_{HI} \simeq 14.8 \text{ cm}^{-2}$ often show associated metal line absorption, but as is seen in Figure 9, there is no such absorption at -82 km s^{-1} . Finally, for the absorption to be hydrogen and not deuterium, its position would have to agree with that of deuterium to within 1 km s^{-1} . Taken together, these arguments indicate that the observed absorption is deuterium, and not hydrogen, but we can not quantify this because we do not know the properties of components of Lyman limit systems.

The scenario in which the absorption is metal line contamination is even less likely for a number of reasons. Any metal lines with a column density of $\log N_{metal} \simeq 14.8 \text{ cm}^{-2}$ would show absorption in not only that ion, but many others along with strong associated hydrogen absorption, some of which would be easily observed in our spectrum, but were not. Also, for the observed absorption to be entirely derived from metal line contamination, such metal lines would have to appear in 5 different regions of the spectrum, all at positions within approximately 1 km s^{-1} of the predicted positions of deuterium, and with line strength scaling as the oscillator strengths expected for the deuterium Lyman series. A similar argument can be used to exclude the case whereby the absorption at the position of deuterium was hydrogen, but not in the corresponding Lyman series transition (e.g., the absorption at Ly-6 is an unrelated Ly α line).

6. Elemental Abundances and Ionization State of the $z \simeq 2.536$ Lyman Limit System

Here we discuss the abundances of the elements observed in the $z \simeq 2.536$ Lyman limit system which shows D/H.

The general procedure for determining the elemental abundances is to use an ionization model to convert from the observed column densities of selected ions into elemental abundances. On the whole, the level of ionization in QSO absorption line systems tends to decrease as the column density of the gas increases, since the gas can shield itself more from ionizing Lyman continuum radiation. Typical Lyman limit systems with $\log N_{HI} \simeq 17.5 \text{ cm}^{-2}$ are highly ionized, whereas damped Ly α systems, whose column densities are greater than $\log N_{HI} = 20 \text{ cm}^{-2}$ are typically neutral. In the case of HS 0105+1619, we expect the gas to be predominantly neutral ($\text{H I}/\text{H} \geq 0.5$), since the column density is approaching that of a damped Ly α system.

6.1. Ionization & Metallicity

We modeled the ionization with the CLOUDY v90.04 package developed by G. Ferland (Ferland, 1991). As usual, we assumed a plane-parallel geometry with constant density $n_H = 0.01 \text{ cm}^{-3}$, and we approximated an isotropic background ionizing radiation by placing a point source at a very large distance. We used the Haardt-Madau ionizing spectrum (Haardt & Madau, 1996). In Figure 11 we show the correction which would be added onto an observed ionic abundance to give an elemental abundance: $[\text{X}/\text{H}] = \log(N_X/N_{HI}) + \log \epsilon(\text{X}/\text{H I}) - \log(\text{X}/\text{H})_{\odot}$, where N_X is the column density of the ion used to infer the abundance of element X . Since we hold the N_{HI} , the gas density and the spectrum constant, these corrections are specified in terms of the intensity of the ionizing flux at 1 Ryd, $\log J_{912}$. Because the corrections are nearly homologous with the ratio n_H/J_{912} , we can account for different n_H values by simply shifting J_{912} .

For the D/H absorber, we can obtain the $[\text{O}/\text{H}]$ without ionization correction, because we have four un-blended O I transitions which give the most accurate N_{OI} in any absorption system to date. The ionization correction for O I is negligible, $\log \epsilon(\text{O I}/\text{H I}) < 0.2 \text{ dex}$, even at extreme values of J_{912} , and O I/H I is equal to O/H, which gives $[\text{O}/\text{H}] = -2.0$.

This abundance is supported by four other elements. Figure 11 shows that the ionization corrections for Si II, C II, Al II, and Fe II are all negative. Therefore, we can place upper limits on the C, Si, Fe, and Al abundances

using the observed C II/H I, Si II/H I, Fe II/H I and Al II/H I ratios without corrections. We find $[C/H] \leq -1.9$, $[Al/H] \leq -2.1$, $[Fe/H] \leq -1.9$, and $[Si/H] \leq -1.85$, all within 0.15 dex of $[O/H]$. Note that these elements might have shown different abundances, because they are seen in lines which have different velocities and velocity widths from the H I, D I and O I. From N I, we find $[N/H] \simeq -3.1$ without ionization correction, as suggested by the other elements. This implies that N is under-abundant by approximately 1.1 dex, which is not unusual for damped Ly α systems with similarly low metal abundances (Centurion et al. 1998; Lu, Sargent & Barlow 1998), but is much more N than usual in Galactic and extra-galactic H II regions (Henry, Edmunds & Köppen 2000).

The similarity of these abundance values shows that each element is primarily in the listed ion, O I, Si II, Fe II, Al II and C II, and that $H\text{ I}/H > 0.8$. This low ionization requires $(J_{912}/10^{-21} \text{ erg cm}^{-2} \text{ s}^{-1} \text{ Hz}^{-1} \text{ sr}^{-1}) (10^{-2} \text{ cm}^{-3}/n_H) < 1$, and hence a weak radiation intensity and high gas density. When we divide the N_{HI} by the gas density, we find that size of the cloud along the line of sight would be $l < 1$ kpc, assuming a homogeneous medium. If the absorbing region were spherical, its gas mass would be $< 1.2 \times 10^5 M_{\odot}$.

The observed Si III, C III, C IV or Si IV absorption must come from separate, more highly ionized gas.

7. Best Fit Values for HS 0105+1619

For the gas giving D/H in HS 0105+1619, the best values for various parameters, and the 1σ errors, are as follows:

- $\log N_{HI} = 19.422 \pm 0.009 \text{ cm}^{-2}$ (2% error)
- $\log N_{DI} = 14.826 \pm 0.039 \text{ cm}^{-2}$ (9% error)
- $\log D/H = -4.596 \pm 0.040$ (10% error)
- $D/H = 2.54 \pm 0.23 \times 10^{-5}$
- temperature: $T = 1.15 \pm 0.02 \times 10^4 \text{ K}$
- Gaussian turbulent velocity width: $b_{turb} = 2.56 \pm 0.12 \text{ km s}^{-1}$
- log oxygen abundance, on the solar scale: $[O/H] = -2.0$
- other limits: $[C/H] \leq -1.9$, $[Al/H] \leq -2.1$, $[Fe/H] \leq -1.9$, $[Si/H] \leq -1.85$, $[N/H] \simeq -3.1$
- neutral fraction: $H\text{ I}/H > 0.8$

- gas density: $n > 0.01 \text{ cm}^{-3}$ (for $J_{912} \geq 10^{-21} \text{ erg cm}^{-2} \text{ s}^{-1} \text{ Hz}^{-1} \text{ sr}^{-1}$)
- extent of absorbing region along the line of sight: $< 1 \text{ kpc}$
- mass of gas: $< 1.2 \times 10^5 M_{\odot}$.

For D/H, we added the errors on $\log N_{HI}$ and $\log N_{DI}$ in quadrature, because we expect little correlation.

8. Best values for D/H from all QSOs

The weighted mean D/H from three QSOs, PKS 1937–1009, Q1009+2956, and HS 0105+1619 (the other QSO, Q0130–4021, gives a consistent upper limit) is $\log D/H = -4.523 \pm 0.026$ (6% error). The individual parameters from our measurements of four QSOs are summarized in Table 5. The dispersion in the three measurements of D/H is larger than expected. We obtain a $\chi_2^2 = 7.1$, which would be exceeded in 3% of random samples with Gaussian errors. There are two interpretations. Either we have under-estimated the errors, or there is real dispersion in D/H. We favor the former interpretation, since there are a number of systematic errors which affect each measurement, and are difficult to assess. For example, we may have under-estimated the effect of contamination in PKS 1937–1009 or Q1009+2956. Hydrogen absorption near the D I lines would artificially increase the D/H estimated for these objects. We now discuss another possible source of scatter in D/H, astration, the destruction of deuterium in stars.

8.1. Primordial Nature of the Gas & Astration

At a metallicity of 0.01 solar, all chemical evolution models which are consistent with Galactic data predict that the destruction of deuterium is about 1%, ten times smaller than our measurement error (Tosi et al. 1998; Jedamzik & Fuller 1997).

We can get an approximate estimate of the amount of deuterium which will have been destroyed in stars by linearly scaling from the local interstellar medium (LISM). Since 50% of the primordial deuterium is lost from the LISM where the metal abundance is approximately 0.7 solar, we expect 0.7% to be lost at 0.01 solar. This scaling is only approximate for many reasons: the relation is not linear in the LISM today because the destruction is saturating, there has been infall of less processed gas, and the high mass stars which we expect polluted the absorption systems destroy less deuterium for a given amount of

metal production.

We now discuss the relation between the D/H values and the metallicity which we have measured towards QSOs. The D/H values for the four QSOs listed in Table 5 range from $< 6.7 \times 10^{-5}$ to 2.54×10^{-5} , while the [Si/H] ranges from -2.6 to -1.85 . Figure 12 shows that these values appear correlated, in the sense that the D/H is lower when the metallicity is higher. This is the sense expected if the deuterium has been destroyed in those absorbers with higher metallicity. The D/H for Q1009+2956, PKS 1937–1009 and HS 0105+1619 appears to decline linearly with increasing [Si/H]. The D/H declines by a factor of 0.64 between Q1009+2956 and HS 0105+1619 while the [Si/H] increases from approximately -2.53 to -1.85 .

There are two arguments against the reality of the correlation. First, we do not expect such a large destruction of deuterium when the metal abundance remains this low. A decrease in the D/H by a factor of 0.64 implies that 0.64 of the atoms in the absorbing gas have not been in a star, and that 0.36 have been in one or more stars, which is at least an order of magnitude more than expected. Second, the indicated rate of decrease of the D/H is much faster than expected. We expect D/H to decrease linearly with the linear, and not log, metal abundance.

Models of the evolution of the chemical abundances in our Galaxy predict that D/H will remain near the primordial value – a horizontal straight line on Figure 12 – for [Si/H] < -1 (Prantzos 1996, Fig. 4b; Prantzos & Silk 1998, Fig. 3; Matteucci, Romano & Molaro 1999, Fig. 7b). The D/H declines at higher abundances, because a significant fraction of the atoms in the ISM have then come from within stars. The abundance at which the D/H decline becomes significant depends on the details, including the element used to gauge the metal abundance, the amount of that element ejected from stars, the fraction of the H in the ISM which has not been inside a star, the infall of gas with abundances nearer to the primordial values, and the amount of mixing.

The Galactic chemical evolution models apply on average to large volumes of gas which are well mixed. At the epoch of observation the gas may instead be isolated, and the elemental abundances may have been determined by relatively few stars. This will allow more stochastic variation in the D/H at a specific metal abundance, but it will not change the general expectation that D/H will remain near the primordial value as long as the metal abundances are low.

9. New Values for the Relevant Cosmological Parameters

We take the weighted mean of the D/H values from three QSOs, PKS 1937–1009, Q1009+2956 and HS 0105+1619, as our best estimate for the primordial D/H ratio. We include all three QSOs because we believe that the dispersion in these D/H values is dominated by systematic errors. We weight by the quoted errors, which we believe indicate the relative sizes of the random errors. For the error on the best value of D/H we take the dispersion in the three values, divided by $\sqrt{3}$. We do not use the error on the weighted mean, which is unrealistically small, because the dispersion on the values is larger than expected. We then estimate:

- $\log D/H = -4.52 \pm 0.06$ (15% error), or
- $D/H = 3.0 \pm 0.4 \times 10^{-5}$.

This new D/H value, together with over 50 years of theoretical work and laboratory measurements of reaction rates, leads to the following values for cosmological parameters (Esposito et al 2000a,b; Burles, Nollett & Turner, 2000):

- $\eta = 5.6 \pm 0.5 \times 10^{-10}$ (from standard BBN and D/H)
- $\Omega_b h^2 = 0.0205 \pm 0.0018$ (baryon density, in units of the critical density, 9% error)
- $Y_p = 0.2471 \pm 0.0009$ (predicted mass fraction of ${}^4\text{He}$, from SBBN and D/H)
- ${}^3\text{He}/\text{H} = 1.09 \pm 0.06 \times 10^{-5}$ (predicted from SBBN and D/H)
- ${}^7\text{Li}/\text{H} = 3.8_{-0.8}^{+1.0} \times 10^{-10}$ (predicted from SBBN and D/H),

where the error on Y_p includes the error from D/H (0.0008) and from the calculation of Y_p for a given η (0.0004) (Lopez & Turner 1999).

These values are generally consistent with most other measurements (Tytler et al. 2000; Burles, Nollett & Turner 2000; Olive, Steigman & Walker 2000). For example, Pagel (2000) reviews Y_p measurements and concludes that “systematic errors up to about 0.005 are still not excluded”, and that “ Y_p is very probably between 0.24 and 0.25”. Of special note are ${}^7\text{Li}$ and the cosmic microwave background (CMB) estimate of $\Omega_b h^2$.

The predicted value for the ${}^7\text{Li}/\text{H}$ abundance is a factor of two to five times higher than measured in halo stars (Bonifacio & Molaro 1997; Ryan, Norris & Beers 1999). Models allow at most a factor of two destruction of the ${}^7\text{Li}$ in these stars (Ryan et al. 1999, 2000; Deliyannis & Ryan 2000; Tytler et al. 2000).

Recent measurements of $\Omega_b h^2$ from the CMB are in agreement with our value from D/H and SBBN. Compared to our more accurate $\Omega_b h^2$ value, the value from BOOMERANG (Lange et al. 2000: $\Omega_b h^2 = 0.031 \pm 0.004$) is approximately 3σ higher, that from MAXIMA-I (Balbi et al. 2000: $\Omega_b h^2 = 0.025 \pm 0.010$) is 0.5σ higher and that from the Cosmic Background Imager (Padin et al. 2001: $\Omega_b h^2 = 0.009$) is just over 1σ lower. The agreement of these $\Omega_b h^2$ values is a dramatic validation of the physics used in SBBN and CMB.

10. Summary & Discussion

We have presented the fourth quasar, HS 0105+1619, which shows an absorption system having a low deuterium to hydrogen abundance ratio: $D/H = 2.54 \pm 0.23 \times 10^{-5}$ in the $z \simeq 2.536$ Lyman limit absorption system. We first obtained low resolution spectra in our survey for D/H QSOs with the Lick 3 meter Shane telescope, and here we presented over 24 hours of spectra from the HIRES spectrograph on the Keck-I telescope.

The absorber has a high neutral hydrogen column density, $\log N_{HI} = 19.422 \pm 0.009 \text{ cm}^{-2}$ which is 36 times larger than the next highest case studied for D/H, but 8–100 times less than standard damped Lyman alpha systems. Very little is known about absorbers with $\log N_{HI} \simeq 19 \text{ cm}^{-2}$, and this absorber may not be representative of this class because it was selected to have a very simple velocity structure and low b values.

While the absorber towards object has by far the highest neutral H I column density of the absorbers which we have studied for D/H, it also has the lowest total Hydrogen column density, by a factor of 4 – 7, when we correct for the ionization.

We know little about the environment around the absorber. It might be in the outer parts of galaxy, as are LLS at low redshift, or in a disk, as are damped Lyman alpha absorbers at high redshift. Alternatively, it may be in a relatively isolated gas cloud, because see just one component, with an exceptionally small spread of velocities. In either case, numerical simulations of the growth of structure suggest that the absorbing gas has been incorporated into a galaxy by today.

For the first time, we detect deuterium absorption in 5 Lyman series transitions, and determine $\log N_{DI} = 14.826 \pm 0.039 \text{ cm}^{-2}$. We have strong arguments that the observed absorption is indeed deuterium, and not inter-loping hydrogen or metal line absorption.

We observe a number of associated metal line absorbers, from which we

calculate that the gas is warm and neutral. The metallicity of the system is $\simeq 0.01$ times solar, indicating that the measured D/H is representative of primordial D/H.

We argue that HS 0105+1619 offers the most secure detection of D/H to date, and that the D/H ratio determined from all QSOs has been made more secure.

10.1. HS 0105+1619 gives the most secure measurement of primordial D/H

The measurement of primordial D/H towards HS 0105+1619 is more secure than our prior measurements towards PKS 1937–1009, Q1009+2956 and Q0130–4021 for several reasons. By secure we mean that we have the most information, and hence there is less chance of undetected errors which might greatly exceed those quoted. We are not explicitly referring to the size of the quoted errors, which are similar for PKS 1937–1009 and HS 0105+1619, and larger for Q1009+2956 .

The absorption system in HS 0105+1619 is simple. Like Q0130–4021, the second most secure result, the absorber in HS 0105+1619 is modeled with a single component, which simplifies the measurement of the column densities. PKS 1937–1009 was modeled with two or three components, and Q1009+2956 with two to four.

HS 0105+1619 is the only case to show more than one strong deuterium line, which reduces the chance of contamination, and gives more reliable b values, and hence N_{DI} .

For HS 0105+1619 we listed above the many reasons why the absorption near the deuterium line position is deuterium. The chance of serious contamination from the Ly α forest will decrease with rising N_{DI} . Such contamination is least likely to be significant in HS 0105+1619, followed by PKS 1937–1009. There is some contamination in Q1009+2956 while for Q0130–4021 we see a lot of contamination, and obtain only an upper limit on N_{DI} . We do not know whether the chance of contamination by components of the Lyman limit system changes with N_{HI} .

We also expect that the chance of contamination decreases as the b value of the deuterium decreases, because H lines often have larger b values. Hence HS 0105+1619 is the most secure detection of deuterium.

For HS 0105+1619 we have the most information on the velocity field and b values because we see several D I, N I and O I lines.

For HS 0105+1619 the metal abundance is obtained with additional redundancy. The gas is nearly neutral, and hence we get the abundances of several elements: H, C, N, O, Al, Fe and Si. For the PKS 1937–1009 and Q1009+2956 we used a standard photoionization model to find the level of ionization which explained the relative abundances of ions such as C II, C III, C IV and Si II, Si III, Si IV. We obtained a solution for each element, and these agreed, which provided a check. For Q0130–4021 the ionization and metal abundances are both less well known.

10.2. The primordial D/H becomes more secure

The new measurement makes the primordial D/H much more secure because in each case we are sampling gas with different physical conditions, and some systematic errors, including those associated with the measurement of column densities, may be different for each QSO. First, the new measurement is the most secure. Second, we have increased the number of QSOs in which we have measured deuterium from two to three. Third, we sample a new region of space. Each absorber is a different direction in the universe, and each samples a sight line of about 1 – 10 kpc, which requires about $10^5 - 10^6$ solar masses of gas. Fourth, the absorbing gas covers a factor of 240 range in N_{HI} . Fifth, the absorption systems have differing ionization, with a range of 2000 in the H I/H ratio.

There is less variation in other parameters. The metal abundances cover a factor of ten, which is the typical for QSO absorption line systems, while the redshifts cover most of the range observable from the ground.

11. Acknowledgments

This work was funded in part by grant G-NASA/NAG5-3237 and by NSF grants AST-9420443 and AST-9900842. The flux calibration was funded in part by NAG5-9224.

The spectra were obtained from the Lick Observatory, and the W.M. Keck observatory, which is managed by a partnership among the University of California, Caltech and NASA.

D.T. thanks Elizabeth Flam for hosting a visit to the Institut de Astrophysique in Paris.

We are grateful to Steve Vogt, the PI for the Keck HIRES instrument which enabled our work on D/H, and to the W.M. Keck Observatory staff;

the observing assistants Joel Aycock, Teresa Chelminiak, Gary Puniwai, Ron Quick, Barbara Scheafer, Cynthia Wilburn, Chuck Sorenson, Terry Stickel and Wayne Wack, and the instrument specialists Tom Bida, Randy Campbell, Bob Goodrich, David Sprayberry and Greg Wirth. We are especially grateful to H.J. Hagen, D. Engels and D. Reimers for sending us information on this QSO prior to publication. We also thank Scott Burles, Salvatore Esposito, Craig Hogan, Sergei Levshakov, Gianpiero Mangano, Gennaro Miele, Ofelia Pisanti, Tony Readhead, Gary Steigman, Mike Turner and Ned Wright for useful discussion and comments.

REFERENCES

- Adams, T.F., *Astron. Astrophys.* **50**, 461, (1976).
- Burles, S. & Tytler, D., *Astron. J.* **114**, 1330 astro-ph/9707176 (1997).
- Balbi, A. et al. 2000, preprint, astro-ph/0005124
- Bonifacio, P. & Molaro, P. 1997, *MNRAS*, **285**, 847
- Burles, S. & Tytler, D. 1998a, *ApJ*, **499**, 699
- Burles, S. & Tytler, D. 1998b, *ApJ*, **507**, 732
- Burles, S., Nollett, K. & Turner, M. 2000, preprint astro-ph/0008495
- Burles, S., Nollett, K. & Turner, M. 2000, preprint astro-ph/0010171
- Centurion, M., Bonifacio, P., Molaro, P. & Vladilo, G. 1998, *ApJ* **509**, 620
- Deliyannis, C.P. & Ryan, S.G. 2000 *Bull AAS* 196.0602
- Esposito, S., Mangano, G., Miele, G. & Pisanti, O. 2000a, *Nucl. Phys. B* **568**, 421
- Esposito, S., Mangano, G., Miele, G. & Pisanti, O. 2000b, astro-ph/0005571
- Ferland, G. J. 1991, Ohio State Internal Report 91-01
- Haardt, F. & Madau, P. 1996, *ApJ*, **461**, 20
- Hagen, H.J., Engels, D., & Reimers, D. 1999, *A&AS*, **134**, 483H
- Henry, R.B.C., Edmunds, M.C., Köppen, J. 2000 *ApJ* 541 660
- Jaffe, A.H. et al. 2000, preprint, astro-ph/0007333
- Jedamzik, K. & Fuller, G.M. 1997, *ApJ*, **483**, 560
- Kim, T-S., Hu, E.M., Cowie, L.L. & Songaila, A. *AJ* **114**, 2 (1997)
- Kirkman, D., and Tytler, D. 1997, *ApJ*, **484**, 672

- Kirkman, D., Tytler, D., Burles, S., Lubin, D., & O’Meara, J.M. ApJ **529**, 655–660, (2000) astro-ph/9907128
- Kolb, E.W., and Turner, M.S., “The Early Universe”, (Addison Wesley 1990).
- Lange, A.E. et al. 2000, preprint, astro-ph/0005004
- Levshakov, S.A., Kegel, W.H., & Takahara, F., Astron. Astrophys., **336**, L29 astro-ph/9801108 (1998).
- Levshakov, S.A., Agafonova, I.I., Kegel, W.H. 2000, A&A, **360**, 833-845 astro-ph/0003078
- Levshakov, S.A., Agafonova, I.I., & Kegel, W.H. 2000, A&A **355**, L1 astro-ph/9911261
- Levshakov, S.A., Tytler, D. & Burles, S. 2000, in *Early Universe: Cosmological Problems and Instrumental Techniques* proceedings of the Gamov Memorial Intern. Conf. St. Petersburg, Aug 23-28 1999, and Astr. & Astrophysics Trans., vol. 19, No. 3-4, pp. 385-396, Dec 2000, astro-ph/9812114
- Linksy, J. 1998, Space Science Reviews, **84**, 285
- Lopez, R. & Turner, M.S. 1999, Phys. Rev. D. **59**, 103502
- Lu, L., Sargent, W.L.W. & Barlow, T. 1998, AJ, **115**, 55
- Matteuci, F., Romano, F. & Molaro, P. 1999 A& Ap, **341**,458
- Molaro, P., Bonifacio, P., Centurion, M., & Vladilo, G. 1999, preprint, astro-ph/9908060
- Nollett, K.M. & Burles, S. Phys.Rev.D in press astro-ph/0001440 (2000).
- Olive, K.A., Steigman, G. & Walker, T.P. 2000, Phys. Rept., **333-334**, 389
- Padin, S., Cartwright, J.K., Mason, B.S., Pearson, T.J., Readhead, A.C.S., Shepherd, M.C., Sievers, J., Udomprasert, P.S., Holzapfel, S.W.L., Myers, S.T., Carlstrom, J.E., Leitch, E.M., Joy, M., Bronfman, L. & May, J. 2001 ApJL submitted.
- Pagel, B.E.G. 2000, Phys. Rept., **333-334**, 433
- Prantzos, N. 1996 A& Ap, **310**, 106
- Prantzos, N. & Silk, J. 1998 ApJ, **507**,229
- Ryan, S., Beers, T.C., Olive, K.A., Fields, B.D. & Norris, J.E. 2000 ApJ **530**, 57
- Ryan, S., Norris, J.E. & Beers, T.C. 1999, ApJ **523**, 654 astro-ph/9903059

- Savage, B. & Sembach, K. 1996 *Annu. Rev. Astron. Astrophys.* **34**, 279
- Schramm, D. N. & Turner, M. S., *Rev. Mod. Phys.* **70**, 303-318 (1998).
- Suzuki, N. & Tytler, D. 2000, in preparation
- Tosi, M., Steigman, G., Matteucci, F. & Chiappini, C., *Astrophys. J.* **498**, 226 (1998).
- Tytler, D., Fan, X.M., & Burles, S. 1996, *Nature*, **381**, 207
- Tytler, D. & Burles, S., 1997, in *Origin of Matter and Evolution of Galaxies*, eds. T. Kajino, Y. Yoshii & S. Kubono (*World Scientific Publ. Co.*), p.37-63. astro-ph/9606110
- Tytler, D., Burles, S., Lu, L., Fan, X.M., Wolfe, A., & Savage, B.D. 1999, *AJ*, **117**, 63
- Tytler, D., O’Meara, J.M., Suzuki, N., & Lubin, D. 2000, *Physics Scripta*, **60**, in press, astro-ph/0001318
- Vogt, S. S. et al. 1994, *Proc. SPIE*, **2198**, 362
- Walker, T. P., Steigman, G., Schramm, D. N., Olive, K. A. & Kang, H. S. 1991 *ApJ* **376**, 51
- Webb, J. K., Carswell, R. F., Lanzetta, K. M., Ferlet, R., Lemoine, M., Vidal-Madjar, A., & Bowen, D. V. 1997, *Nature*, **388**, 250
- Webb, J. K. 1987, Ph.D. thesis, University of Cambridge
- Wolfe, A. & Prochaska, J. X., preprint, astro-ph/009081

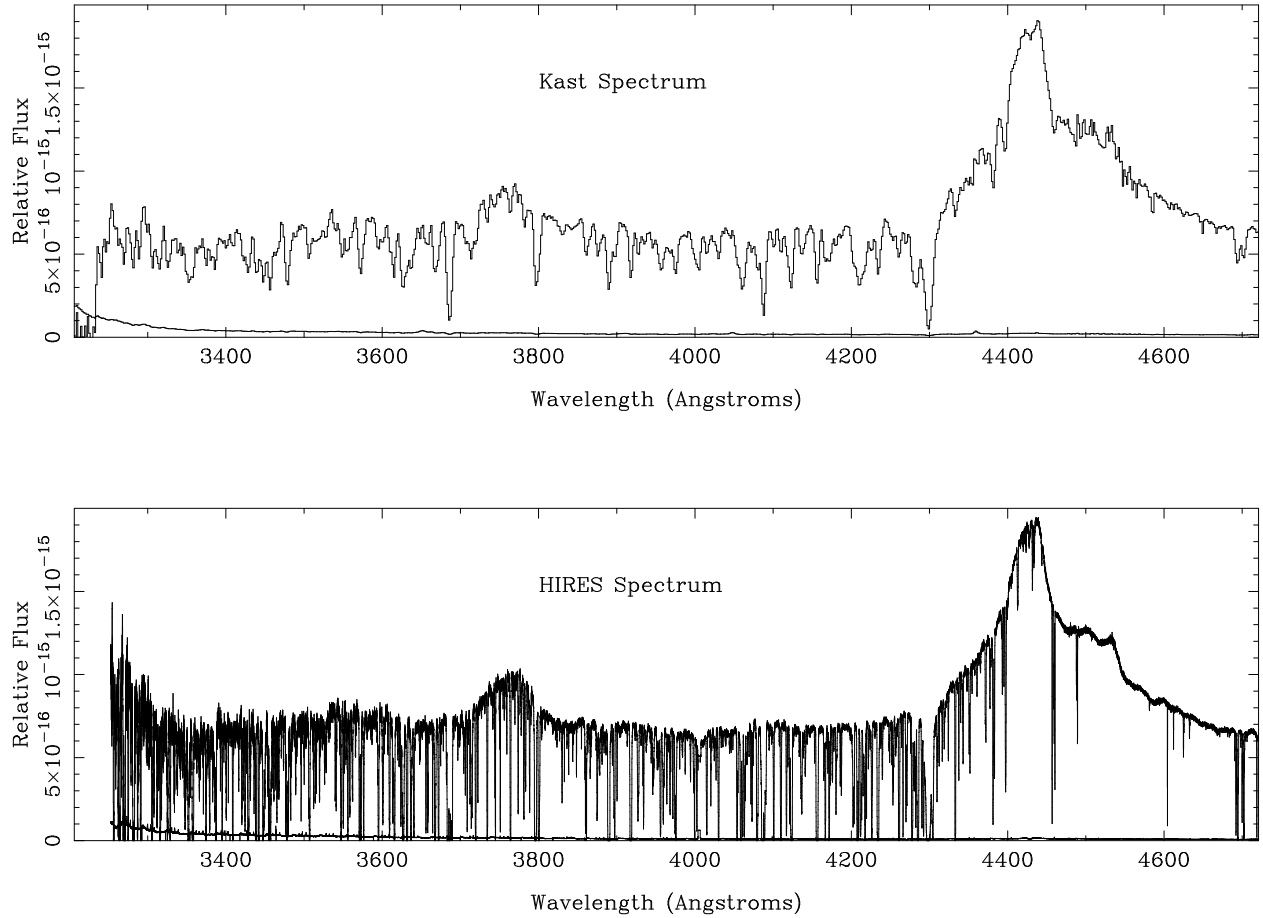


Fig. 1.— Spectrum of HS 0105+1619. The upper panel shows the low resolution flux calibrated spectrum obtained with the Kast spectrograph. The lower panel shows the flux calibrated HIRES spectrum. The flux calibration was noisy at wavelengths less than 3800 Å and was not applied to the Lyman limit, which is not shown above for the HIRES spectrum.

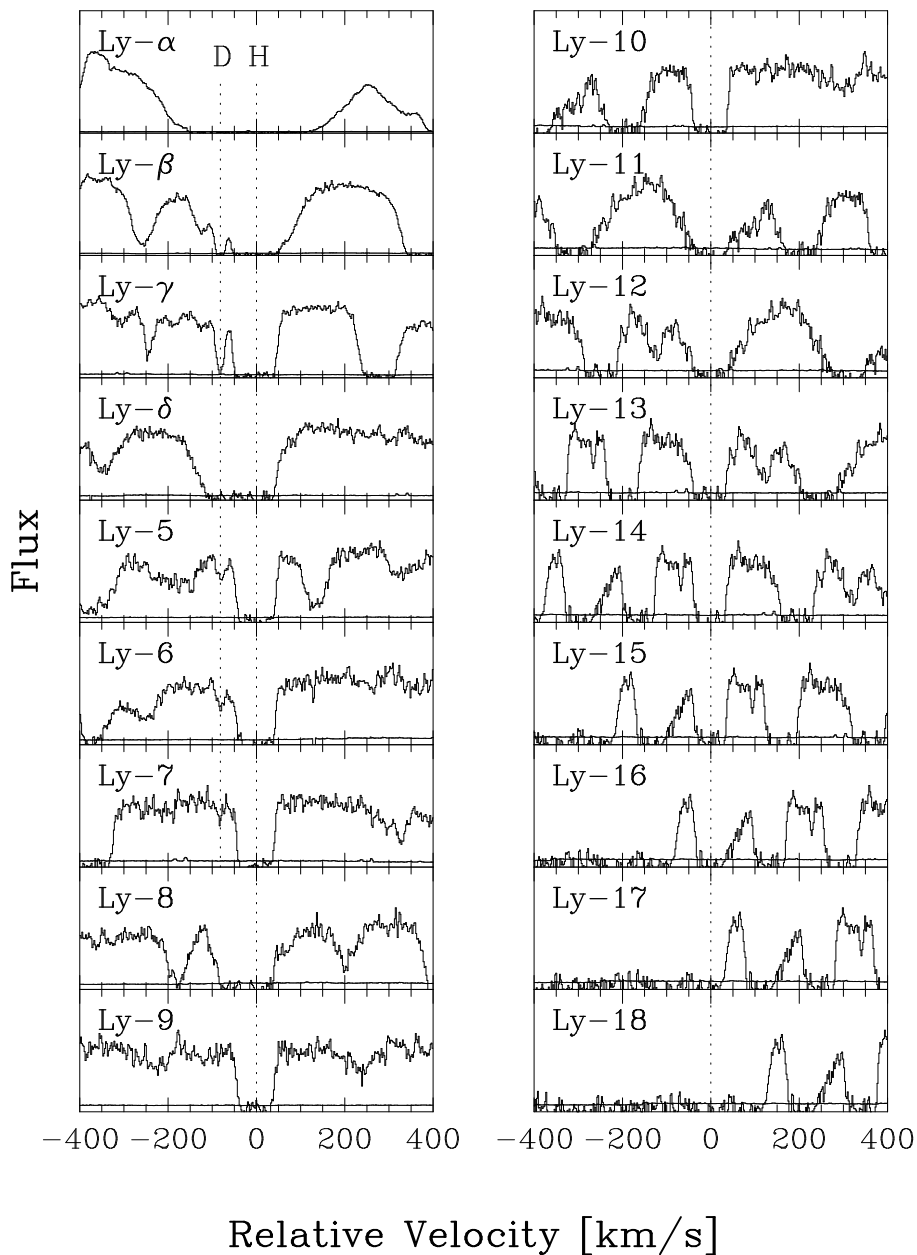


Fig. 2.— Lyman series absorption in the $z \simeq 2.536$ Lyman limit system towards HS 0105+1619. The velocities shown are relative to the H I redshift of $z = 2.535998$. The vertical scales are linear flux, from zero, and the lower traces are the 1σ error. The D I absorption is seen at -82 km s^{-1} in Ly β , Ly γ , Ly-5, Ly-6 and Ly-7.

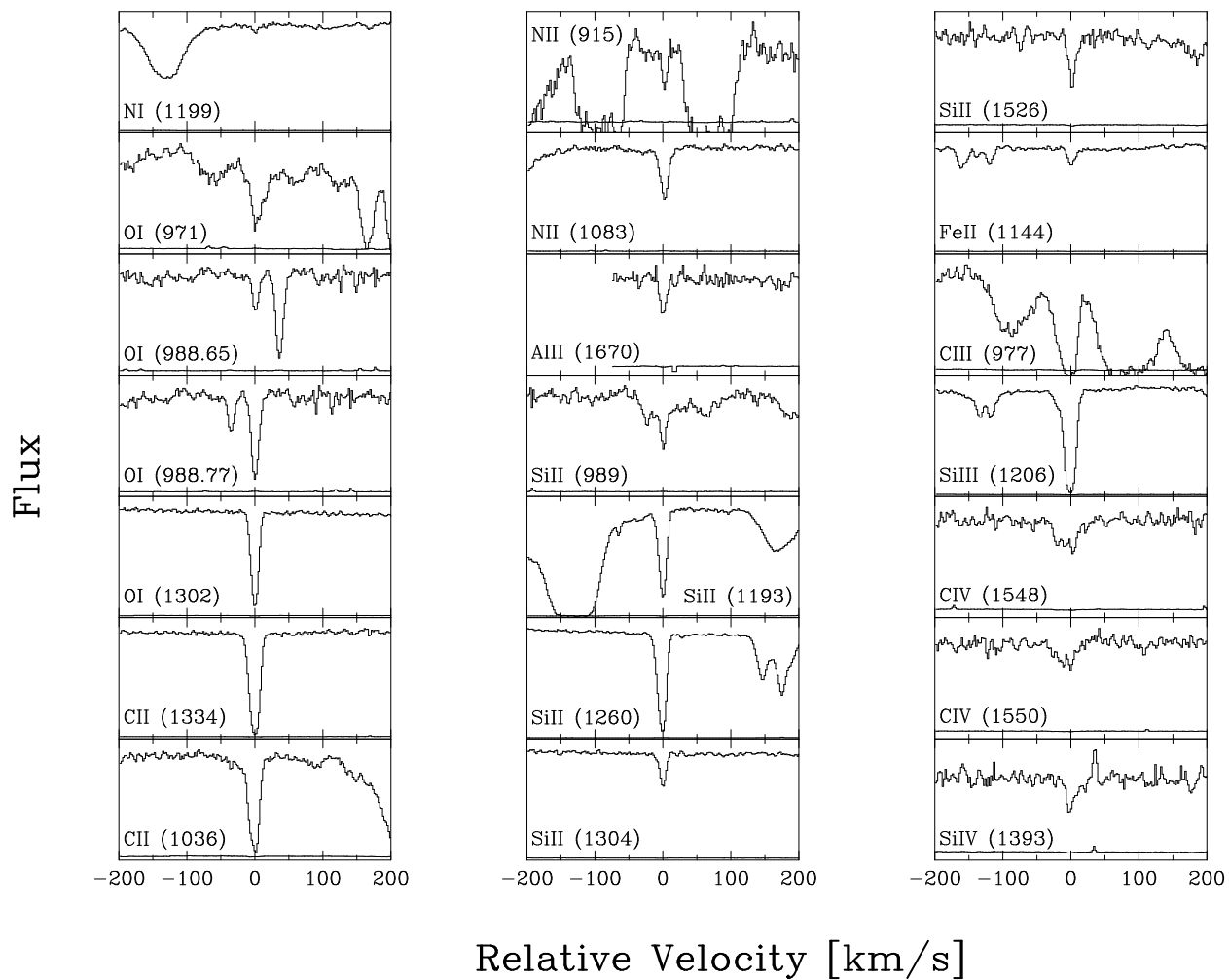


Fig. 3.— Observed metal line absorption associated with the $z \simeq 2.536$ Lyman limit system. The metals are grouped according to ionization state and are organized by atomic mass. The low ionization lines have simple, narrow profiles centered near 0 km s^{-1} .

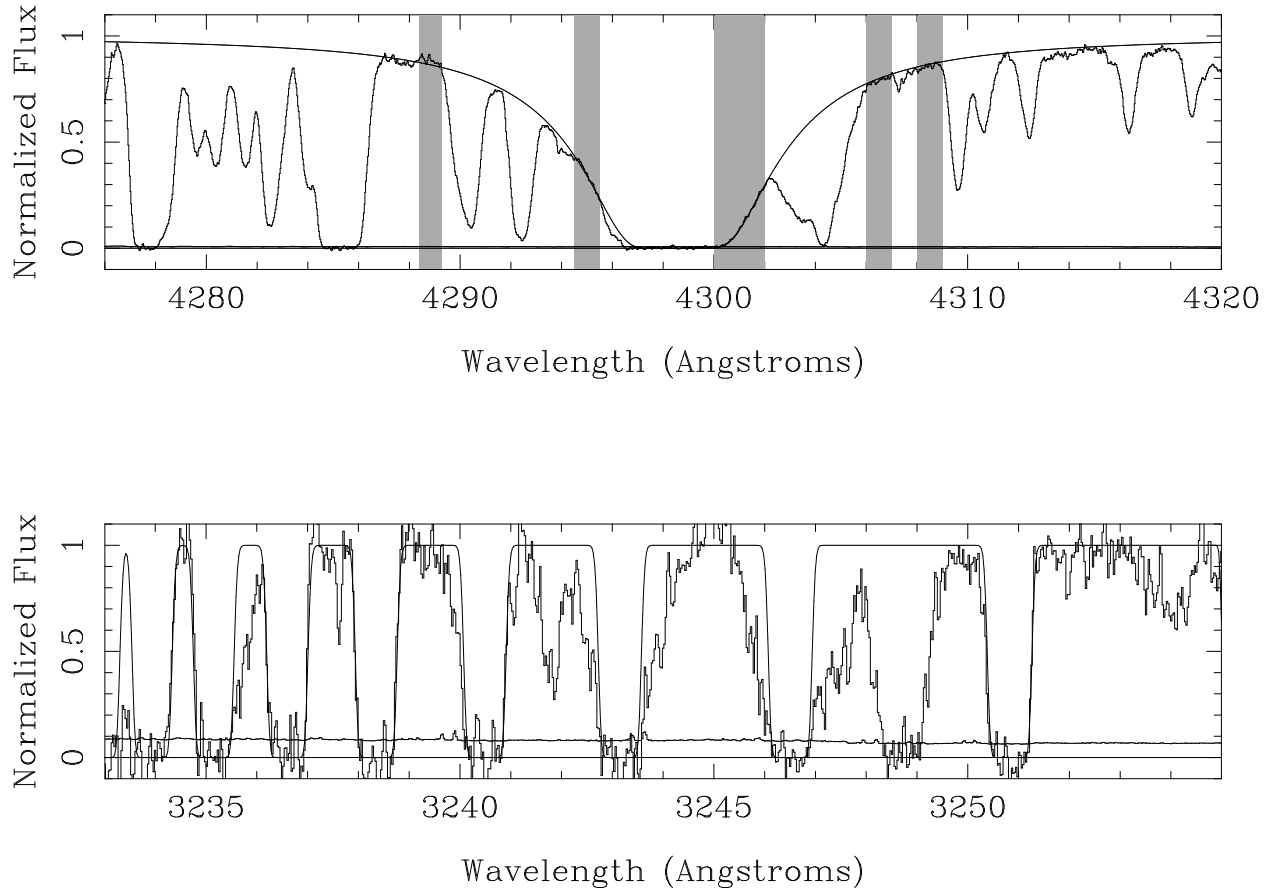


Fig. 4.— Spectral regions used to measure the H I column density. The upper panel shows the Ly α line, with the core and damping wing regions used in the fit shaded grey. The lower panel shows the absorption near the Lyman limit. Over-layed is the single component fit to the hydrogen with a column density of $\log N_{HI} = 19.422 \text{ cm}^{-2}$ from Table 2 .

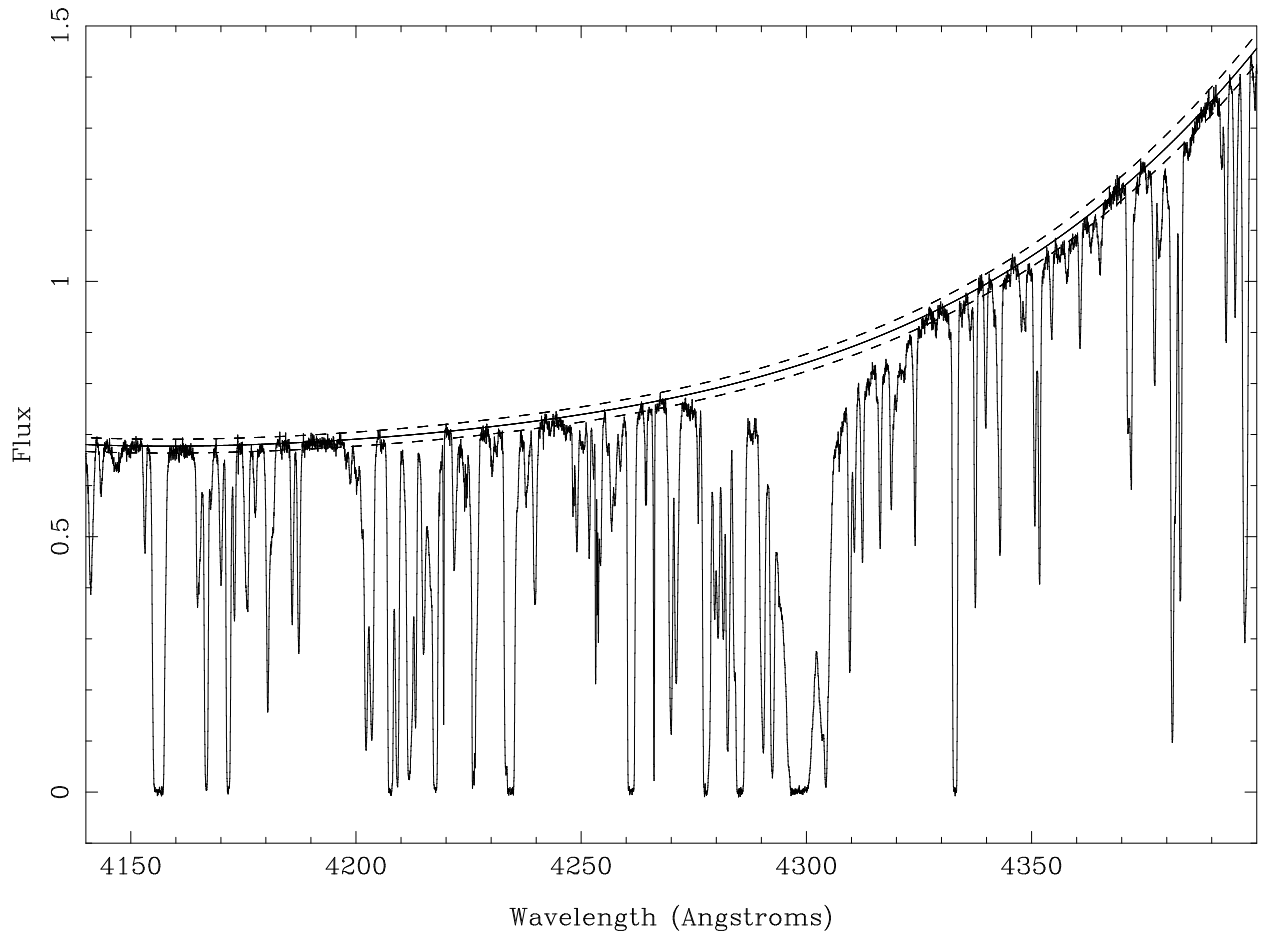


Fig. 5.— Ly α region of the $z \simeq 2.536$ Lyman limit system. Over-layed is the continuum fit (solid line) and the approximate 1σ error to the continuum fit (dashed line).

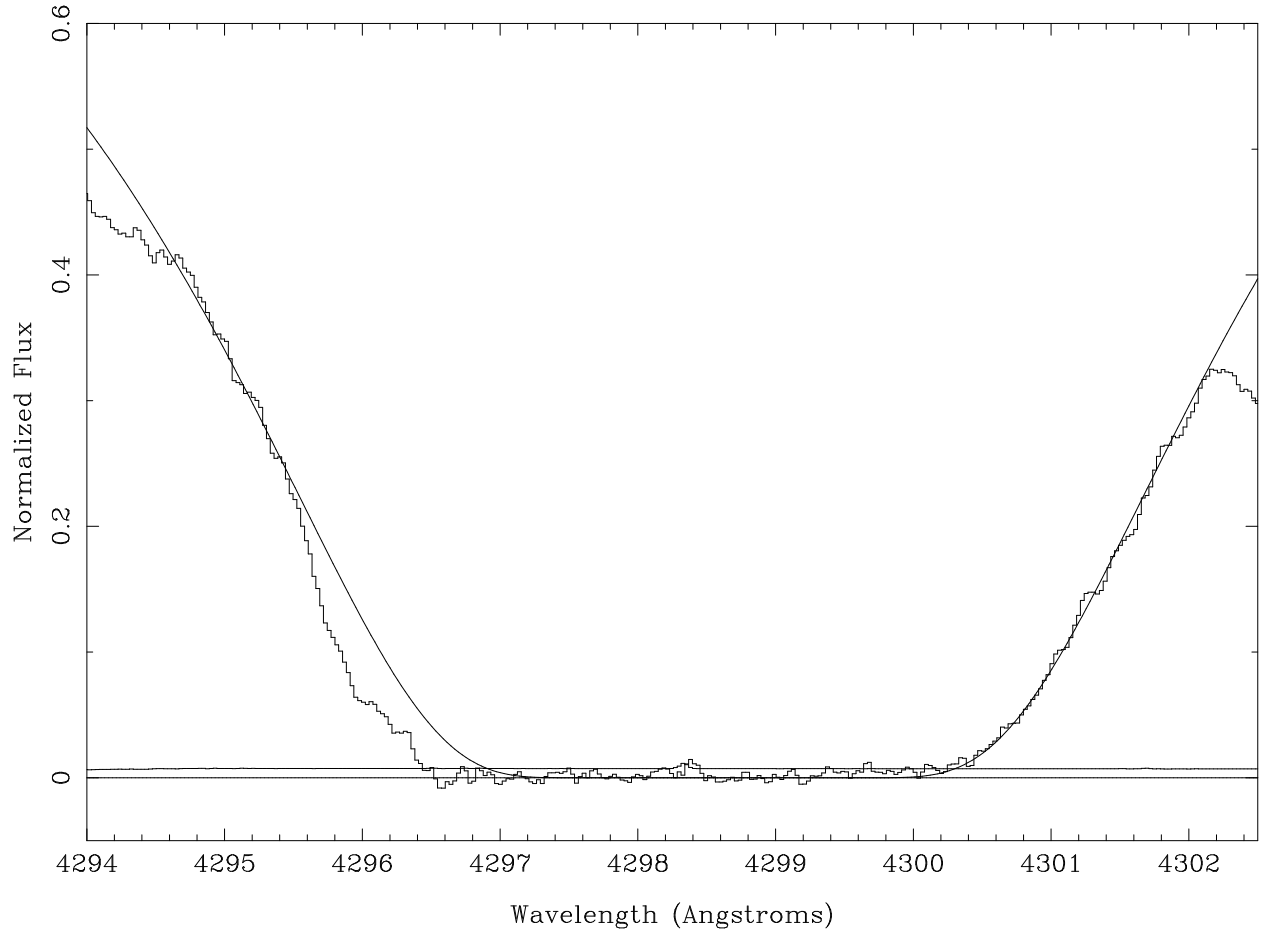


Fig. 6.— Fit to the core region of Ly α with $\log N_{HI} = 19.419 \text{ cm}^{-2}$.

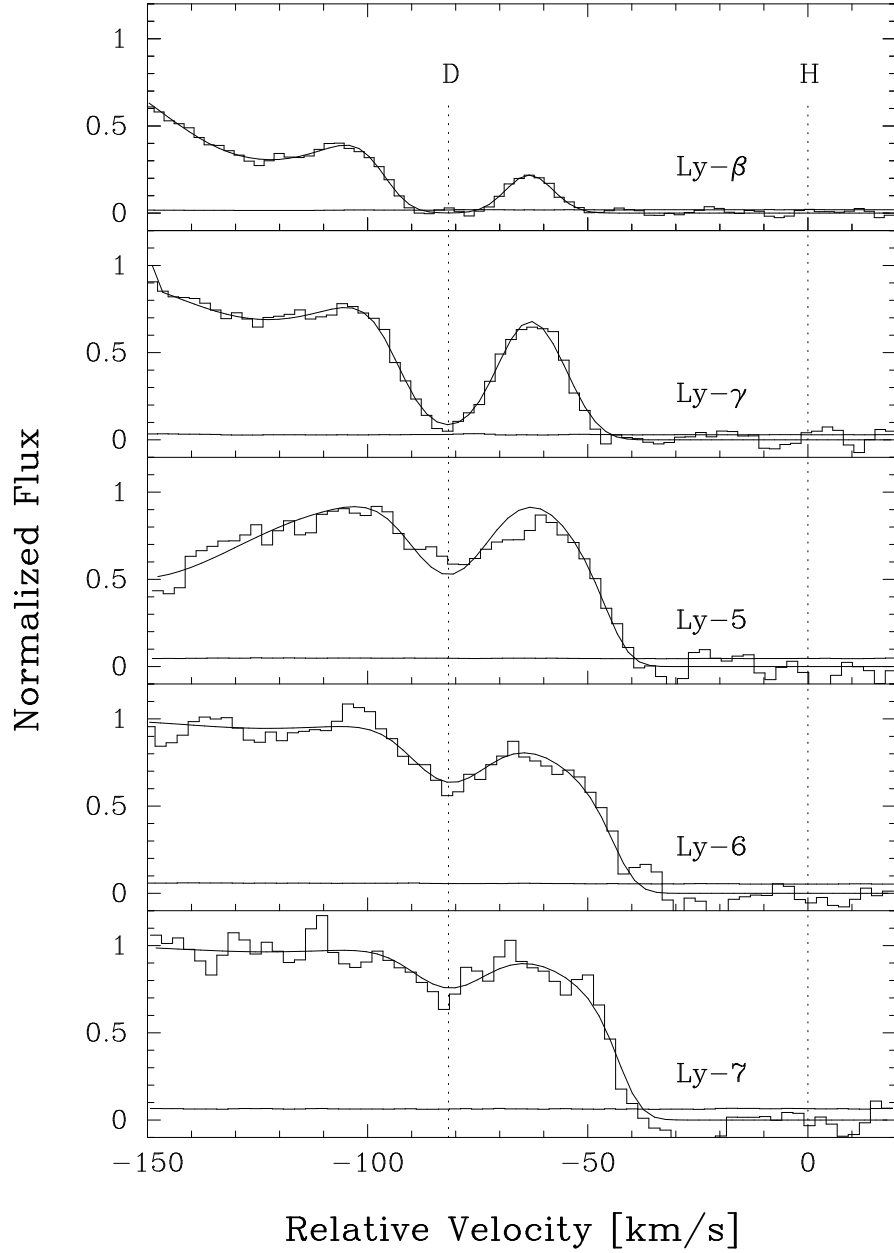


Fig. 7.— Simultaneous fit to the deuterium at -82 km s^{-1} in 5 Lyman series transitions with $\log N_{DI} = 14.81 \text{ cm}^{-2}$ and $b = 9.93 \text{ km s}^{-1}$. Also included in the fit is the H at 0 km s^{-1} and additional Ly α forest absorption.

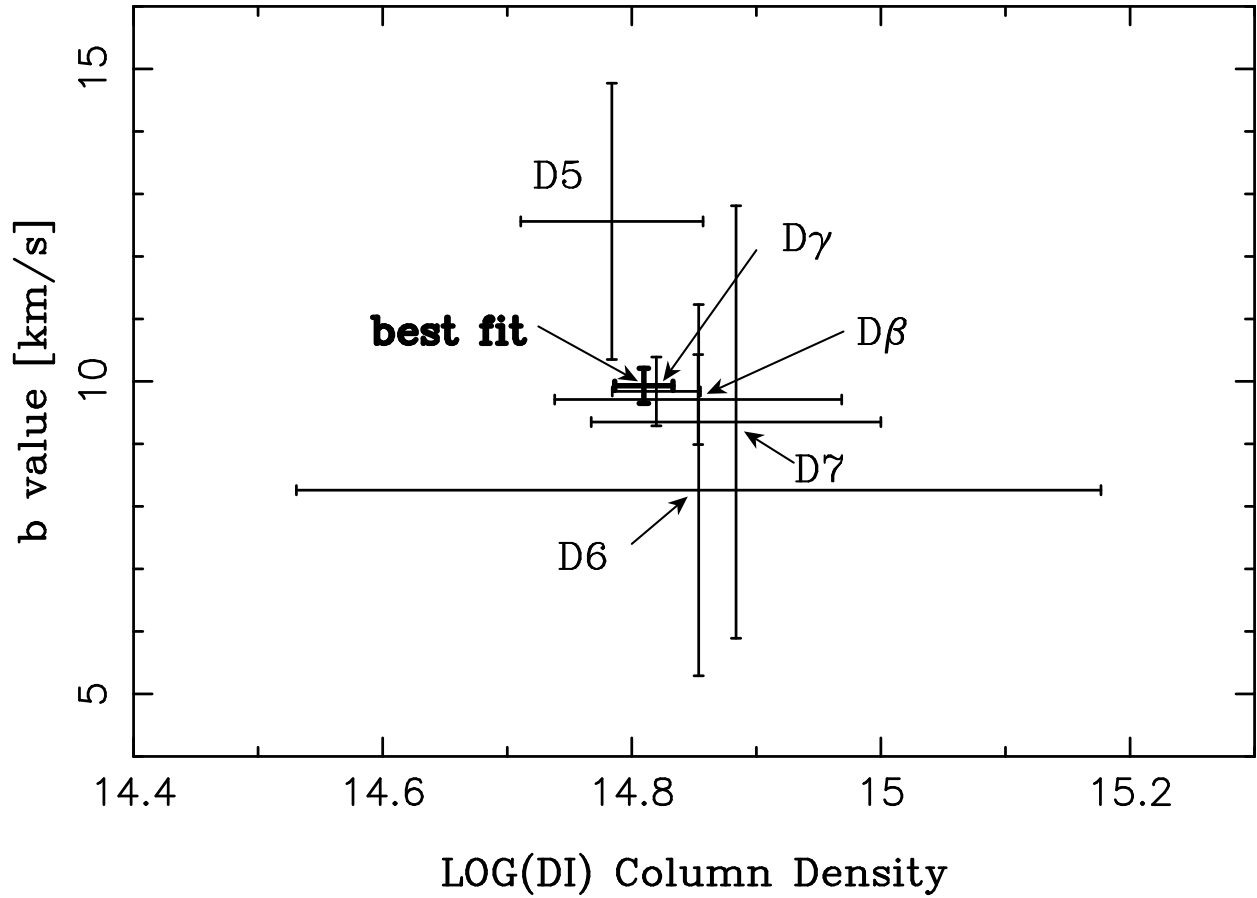


Fig. 8.— Values of the deuterium column density, $\log N_{DI}$ (cm^{-2}), and the absorption width parameter, b , for each of the 5 deuterium lines fit separately. The bold cross represents the values when all lines are fit simultaneously using the best estimate for the continuum level.

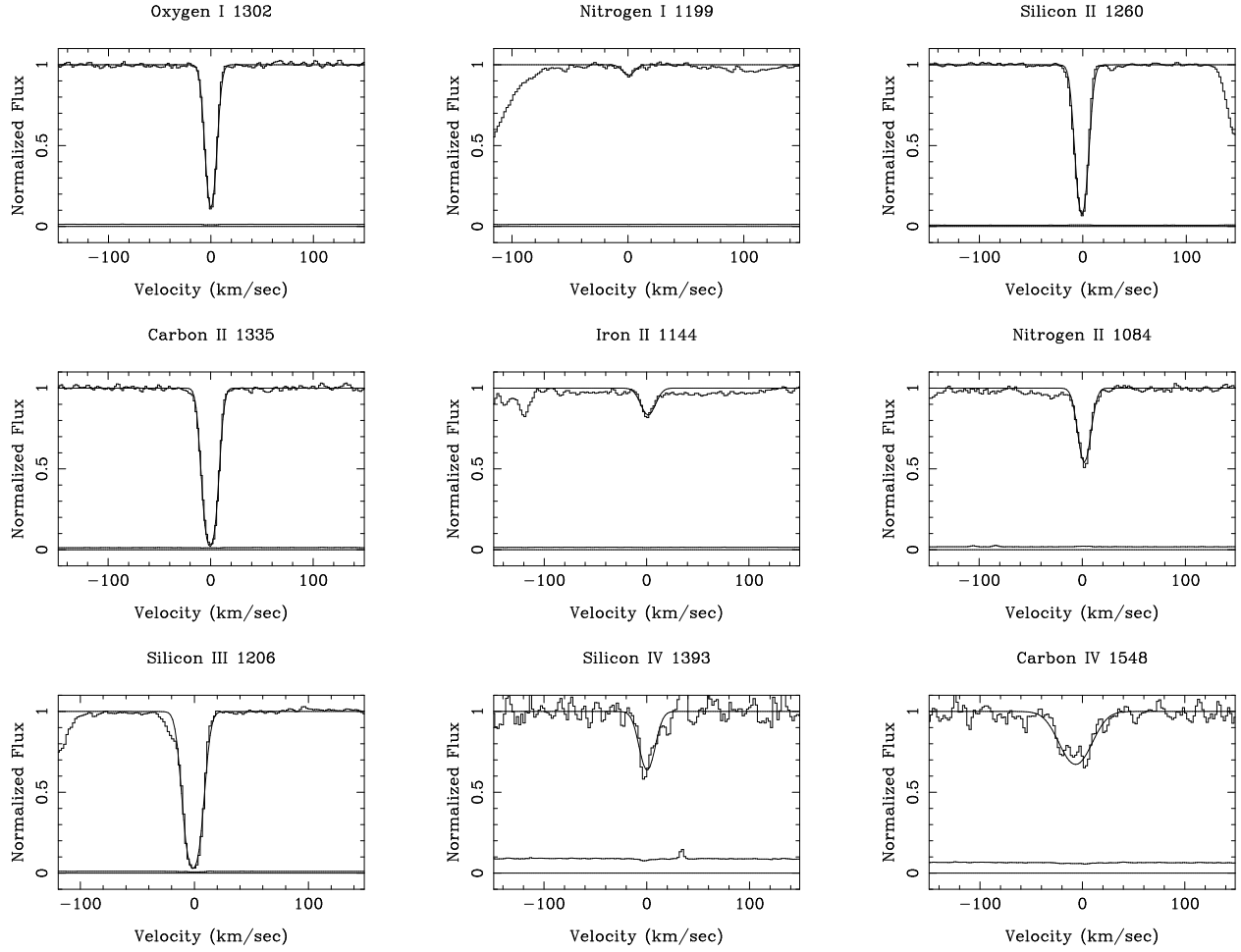


Fig. 9.— Best fit to metal lines associated with the $z \simeq 2.536$ LLS towards HS 0105+1619. The velocities shown are relative to $z = 2.535998$.

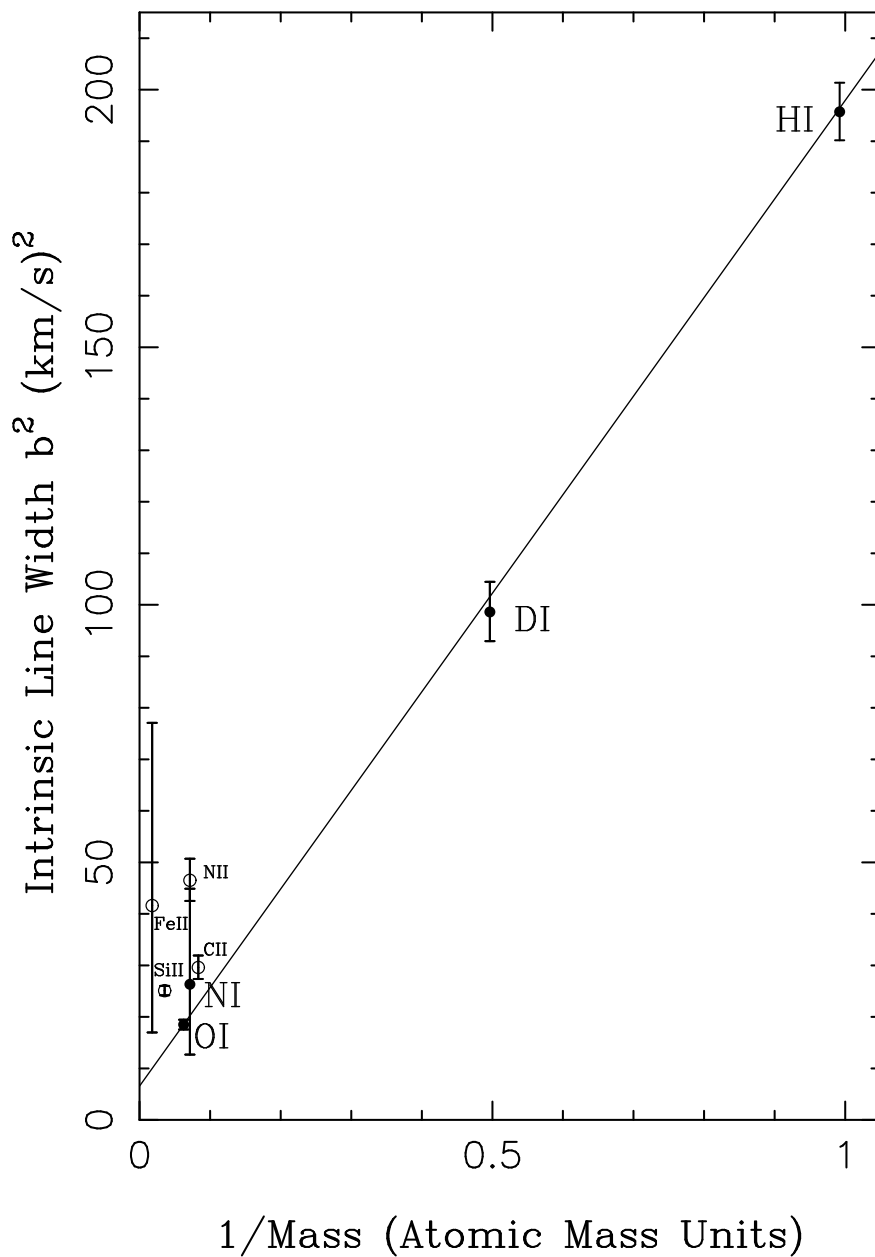


Fig. 10.— Intrinsic velocity widths measured for the neutral and low ionization ions. The straight line is the best fit to H I, N I, and O I alone. The slope of the line gives the temperature of the gas, $T = 1.15 \times 10^4$ K, and the intercept gives the turbulent velocity, $b_{turb} = 2.56$ km s $^{-1}$. The D I absorption comes from the same gas as the H I, N I and O I.

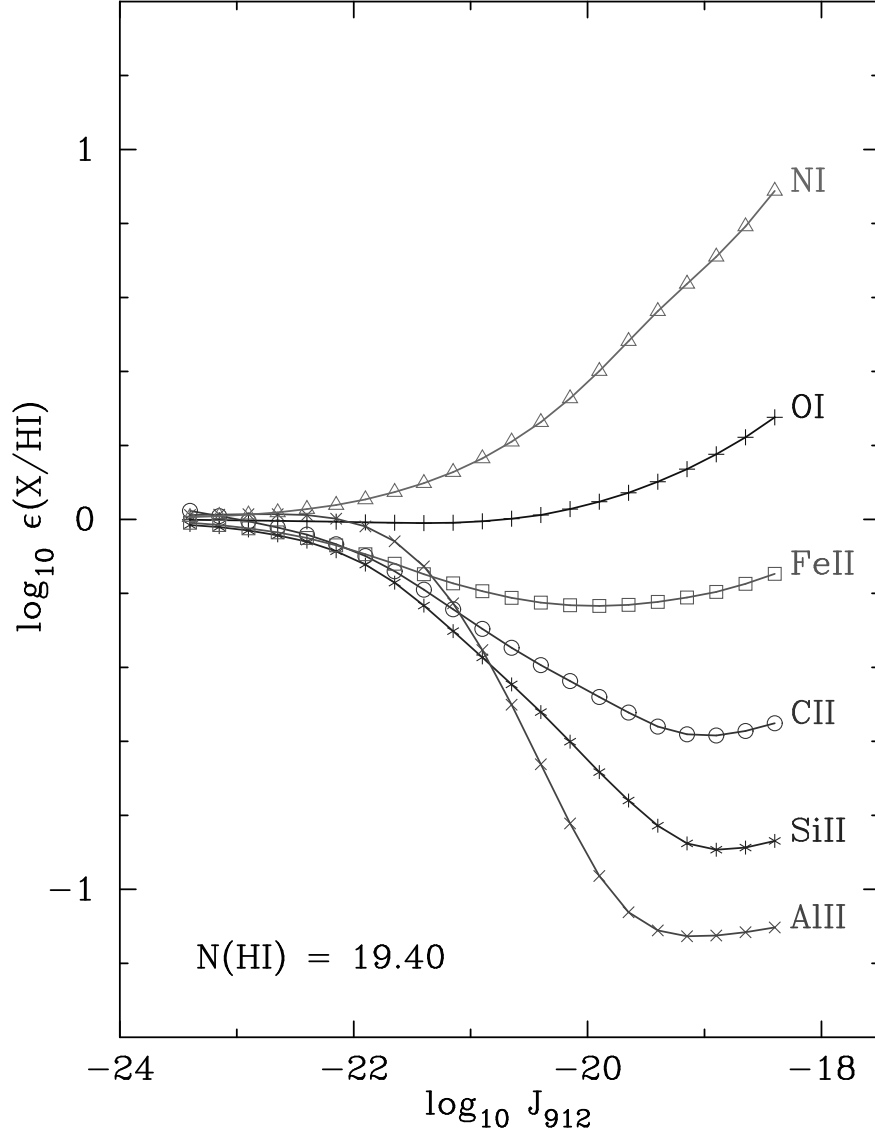


Fig. 11.— The predicted ionization correction $\log \epsilon(X/H I)$ for ion X as a function of the intensity of the photoionizing radiation, $\log J_{912}$, in units of $\text{ergs cm}^{-2} \text{s}^{-1} \text{Hz}^{-1} \text{sr}^{-1}$. We conclude that the ionization is low, as on the left of the plot.

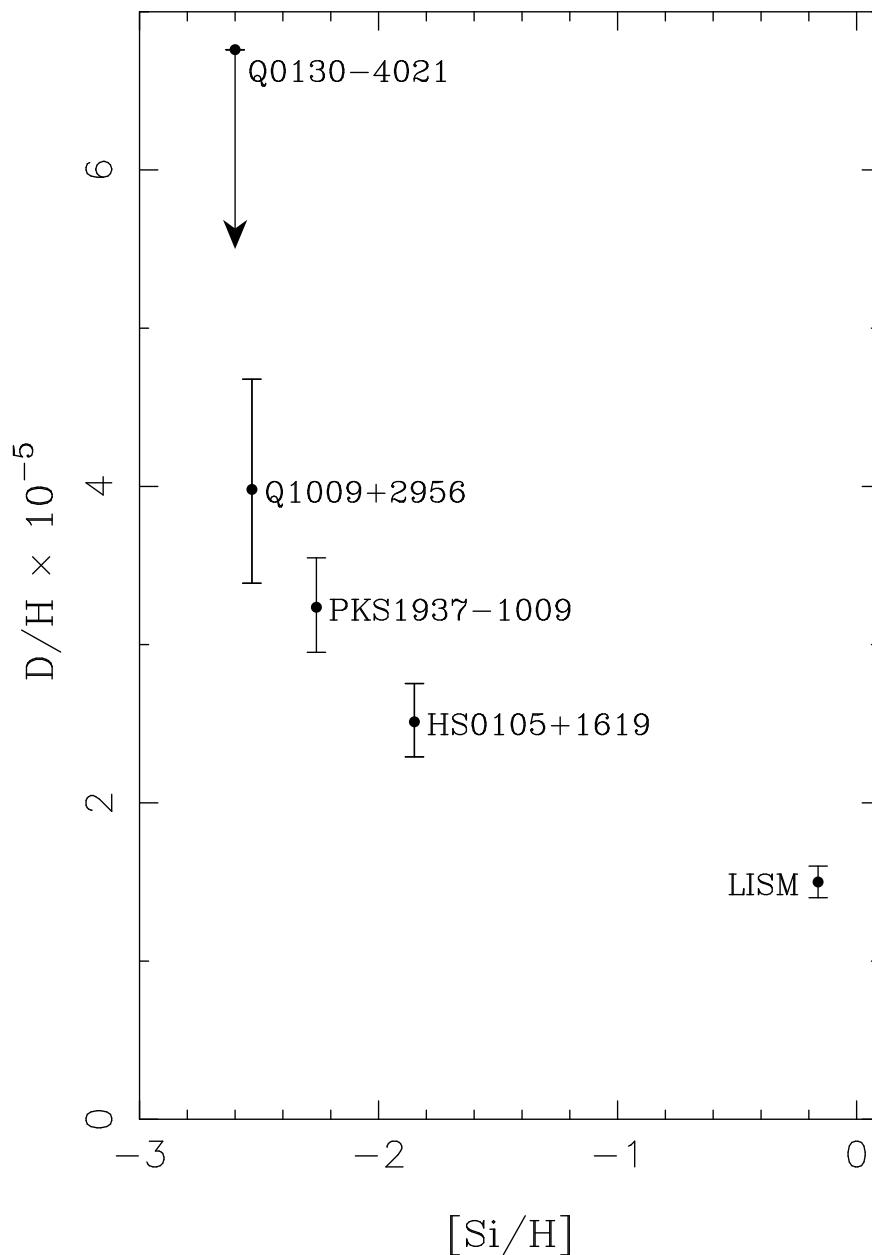


Fig. 12.— The relationship between D/H measurements and metal abundances, as gauged by silicon. Standard chemical evolution models predict little change in D/H until the $[\text{Si}/\text{H}] > -1$, at which time a significant fraction of the gas has come from inside stars, where the D has been destroyed. The values of $[\text{Si}/\text{H}]$ for PKS 1937–1009 and Q1009+2956 represent the mean value, weighted by the total H column density in each component: -2.26 and -2.53 respectively. The D/H value for the local interstellar medium (LISM) is from Linsky (1998), and the LISM $[\text{Si}/\text{H}]$ is from Savage & Sembach (1996).

Table 1. OBSERVATIONS OF HS 0105+1619

Instrument	Date	Integration Time (seconds)	Wavelengths covered (Å)
Kast	August 16, 1998	2700	3200 – 5100
HIRES	October 10, 1999	7200	3200 – 4720
HIRES	October 11, 1999	2×8000	3200 – 4720
HIRES	November 9, 1999	1800	4220 – 6640 ^a
HIRES	September 19, 2000	2×7200	3200 – 4720
HIRES	September 20, 2000	8600, 10800	3200 – 4720
HIRES	September 20, 2000	4×7000	3200 – 4720
Total (HIRES):		86,800	

^aThe wavelength coverage for this observation was not continuous due to 1-10 Å spectral order gaps.

Table 2. IONS OBSERVED IN THE $z \simeq 2.536$ LLS TOWARDS
HS 0105+1619^a

Ion	log N (cm ⁻²)	b^b (km s ⁻¹)	z	v^c (km s ⁻¹)
H I	19.422 ± 0.009 ^d	13.99 ± 0.20	2.535998 ± 0.000007	0.0 ± 0.6 ^e
D I	14.826 ± 0.039 ^f	9.85 ± 0.42 ^f	2.536002 ± 0.000008	0.4 ± 0.7
N I	12.306 ± 0.060	5.13 ± 1.57	2.535998 ± 0.000009	0.0 ± 0.8
O I	14.378 ± 0.024	4.30 ± 0.11	2.535991 ± 0.000001	-0.6 ± 0.1
C II	14.349 ± 0.069	5.44 ± 0.21	2.535985 ± 0.000001	-1.1 ± 0.1
Si II	13.156 ± 0.012	5.01 ± 0.09	2.535980 ± 0.000001	-1.5 ± 0.1
Al II	11.870 ± 0.040	9.69 ± 0.99	2.536019 ± 0.000009	+1.8 ± 0.8
Fe II	12.913 ± 0.087	6.45 ± 2.33	2.535983 ± 0.000014	-1.3 ± 1.2
C III	13.716 ± 0.032	14.48 ± 0.56	2.535923 ± 0.000004	-6.4 ± 0.4
C IV ^g	13.277 ± 0.019	20.40 ± 1.07	2.535913 ± 0.000009	-7.2 ± 0.8
N II	13.501 ± 0.013	6.82 ± 0.30	2.536015 ± 0.000002	+1.4 ± 0.2
Si III	13.097 ± 0.037	7.10 ± 0.24	2.535977 ± 0.000001	-1.8 ± 0.1
Si IV ^g	12.647 ± 0.053	9.16 ± 1.59	2.535995 ± 0.000014	-0.3 ± 1.2

^a The three sections group ions by increasing ionization. For ions in the same gas, we expect the b values to decrease with increasing mass. Errors quoted in the table for the N and z values are from VPFIT alone, except for H I and D I.

^b The intrinsic b value.

^c Velocities are all relative to $z = 2.535998$. The errors in v values come from the errors listed on the z values: $\sigma(v)^2 = (c\sigma(z)/(1+z))^2 + 0.09^2$, where 0.09 km s^{-1} is the minimum internal uncertainty in the wavelength scale. The internal error may be $1 - 2 \text{ km s}^{-1}$, while the external error is approximately $\pm 10 \text{ km s}^{-1}$.

^d The value for $\log N_{HI}$ is the weighted mean from the damping wings and core region of Ly α , and the error includes the continuum level error.

^e The H I z defines $v = 0$. The 0.6 km s^{-1} error is the uncertainty in the v of the H lines in this frame.

^f The N and b for the D I are the weighted means of the individual fits to the five D transitions, and the error on the N includes the contribution from the continuum uncertainty.

^g The lines of this ion may be multiple component blends.

Table 3. SPECTRAL REGIONS USED TO MEASURE D I

Region	λ_{min} (Å)	λ_{max} (Å)
Ly β	3625.1	3627.4
Ly γ	3437.2	3439.2
Ly-5	3314.2	3316.4
Ly-6	3289.4	3291.4
Ly-7	3273.5	3275.2

Table 4. ADDITIONAL LINES USED TO FIT D REGIONS

$\log N$ (cm $^{-2}$)	b (km s $^{-1}$)	z	Region ^a
14.324	25.2	2.53455	all ^b
14.901	18.2	2.53554	all ^b
13.365	26.2	1.72637	Ly-5
12.944	29.7	1.70682	Ly-6
12.770	39.7	1.69376	Ly-7

^aThe regions are defined in Table 3

^bAll D regions used: Ly α , Ly β , Ly γ , Ly-5, Ly-6, and Ly-7

Table 5. PARAMETERS FOR THE D/H MEASUREMENTS

QSO	$\log D/H$	z_{dh}	$\log N_{HI}$ (cm^{-2})	$\log n_{HI}/n_H$	$b(D)$ (km s^{-1})	[Si/H]
PKS 1937–1009 ^a	-4.49 ± 0.04	3.572	17.86 ± 0.02	$-2.35, -2.29$	14.0 ± 1.0	$-2.7, -1.9$
Q1009+2956 ^b	-4.40 ± 0.07	2.504	17.39 ± 0.06	$-2.97, -2.84$	15.7 ± 2.1	$-2.4, -2.7$
Q0130–4021 ^c	< -4.17	2.799	16.66 ± 0.02	-3.4	16 – 23	-2.6
HS 0105+1619 ^d	-4.60 ± 0.04	2.536	19.422 ± 0.009	-0.1	9.85 ± 0.42	-1.85

^a We list the parameters for each of the two components, where available. Results from Tytler, Fan & Burles (1996); Burles & Tytler (1998a).

^b We list the parameters for each of the two components, where available. Results from Tytler & Burles (1997) and Burles & Tytler (1998b).

^cFrom Kirkman et al. (1999).

^dThis paper.